A 10 × 10-Gb/s DFB-LD Array Integrated With PLC-Based AWG for 100-Gb/s Transmission

Oh Kee Kwon, Young-Tak Han, Young Ahn Leem, Jang-Uk Shin, Chul Wook Lee, and Ki Soo Kim

***Abstract*— We describe a hybrid integration module of a 10 × 10-Gb/s distributed feedback laser diode array (DFB-LDA) and a planar light-wave circuit-based arrayed waveguide grating (AWG). For fabrication of the DFB-LDA, we adopted a selective area growth technique to tailor the channel gain properly, and E-beam lithography to accurately control the channel lasing wavelength and grating phase. For implementation of the AWG, we introduced a 2%-Δ structure to reduce the coupling loss between the AWG and DFB-LDA, and designed the tapered and parabolic waveguides at the junctions of the free propagation regions to widen the spectral passband width (i.e., a −1-dB spectral width of 3 nm). The developed module shows a side-mode suppression ratio of >45 dB, a clear eye opening with a dynamic extinction ratio of >4.4 dB at 10 Gb/s, and a power penalty of <1.5 dB after a 2-km transmission for all channels.**

***Index Terms*— 100 Gb/s Ethernet, distributed feedback lasers, laser arrays, arrayed waveguide grating.**

I. Introduction

THE standardization of 100-Gb/s Ethernet (100-GbE) was completed in 2010 [1], and the adoption of 100-GbE Ethernet transceivers has started to grow. In addition, the specifications of 100-GbE multi-source agreement (MSA) were recently proposed and revised for a transmission of 100-Gb/s Ethernet signals over single mode fiber (SMF) with a length of 2 m to at least 2 km, 10 km, or 40 km [2]. The transmitters operating within this specification require the use of ten 1.55-μm light sources separated by an 8-nm wavelength grid operating at a modulation rate of 10 Gb/s.

A ten-channel 10-Gb/s directly modulated distributed feedback laser diode array (DFB-LDA) is considered to be one of the most promising candidates for such a light source. One of the most critical issues in the development of this type of laser array is the performance uniformity over every channel. For example, when we fabricate a multi-channel DFB-LDA employing conventional quantum well (QW) structures, the uniform channel power can be severely limited owing to the relatively narrow gain spectrum (i.e., ∼30 nm). Although many studies have been conducted to implement multi-wavelength DFB-LDAs [3]–[7], with the exception of Ref. [6] and [7], most are focused on the development of dense WDM applications.

Apart from the use of an asymmetric MQW structure [8], the gain spectrum of each channel can also be modified by utilizing the selective area growth (SAG) technique. It was previously reported that a photo-luminescence (PL) spectrum can be red-shifted by 88 nm for a 1.5-μm QW structure without degradation of the spectral quality [9]. From this viewpoint, it is feasible to realize a ten-channel DFB-LDA that can have almost the same optical gain properties for every channel [7]. On the other hand, the fabricated DFB-LDA should be integrated with an optical MUX (or a combiner) for all channel signals to be emitted from one output port. In the hybrid integration of this array structure, the critical issue is the reduction of the coupling loss between the AWG and DFB-LDA and its uniformity over all channels. To do so, it is usually necessary to integrate a spot-size converter into the DFB-LDA. However, this complicates the LD fabrication considerably [10], [11].

In this letter, we fabricate and demonstrate a 10 × 10-Gb/s DFB-LDA integrated with a planar light-wave circuit (PLC) based arrayed waveguide grating (AWG) for application to a 100-Gb/s transmission. For fabrication of the DFB-LDA, the SAG technique, E-beam lithography, and reverse-mesa ridge waveguide (RM-RWG) LD processing are used for properly tailoring the channel gain, accurately controlling the channel lasing wavelength and grating phase (i.e., $\lambda/4$ phase-shift), and effectively reducing the fabrication cost and electrical and thermal resistances, respectively [12]. One output port is realized by the hybrid integration of a DFB-LDA and PLC-based 2%-Δ (index contrast) AWG with wide Gaussian spectral shapes (i.e., −1 dB spectral width of ∼3 nm). The detailed device structure and its transmission properties are reported herein.

II. Design and Fabrication

Fig. 1 shows a photograph of the hybrid integration module composed of a PLC-based ten-channel AWG and a DFB-LDA sub-assembly module. The sub-assembly module contains a ten-channel $\lambda/4$-shifted DFB-LDA, ten surface-mountable device (SMD) resistors, and ten-channel flexible printed circuit board (FPCB) wiring on the copper-tungsten (CuW) metal optical bench (MOB). The DFB-LDA, SMD resistors, and FPCB are die-bonded onto a metalized Si sub-mount, and the module is then chip-to-chip bonded to the AWG. In this

Manuscript received May 20, 2014; revised August 6, 2014; accepted August 13, 2014. Date of publication August 21, 2014; date of current version October 9, 2014. This work was supported by the Energy Efficient Power Semiconductor Technology for Next Generation Data Center, IT Research and Development Project, through the Korea Ministry of Knowledge Economy, Korea Evaluation Institute of Industrial Technology, Seoul, Korea, under Grant 10038766.

The authors are with the Convergence Components and Materials Research Laboratory, Optical/Wireless Convergence Component Research Department, Electronics and Telecommunication Research Institute, Daejeon 305-350, Korea (e-mail: okkwon@etri.re.kr; frenclin@etri.re.kr; leem@etri.re.kr; shju@etri.re.kr; leecw@etri.re.kr; kimks1136@etri.re.kr).

Color versions of one or more of the figures in this letter are available online at http://ieeexplore.ieee.org.

Digital Object Identifier 10.1109/LPT.2014.2349072

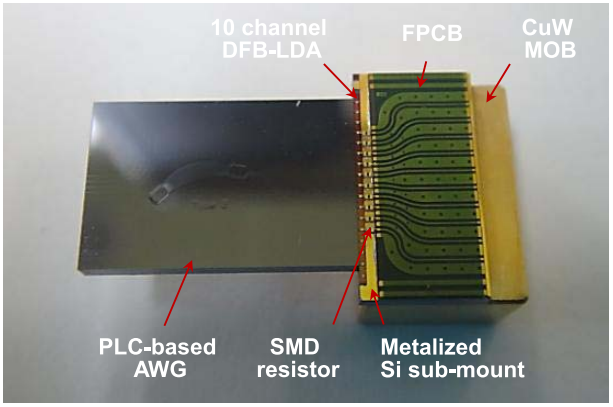

Fig. 1. A photograph of a hybrid integration module of a PLC-based AWG and a DFB-LDA sub-assembly module.

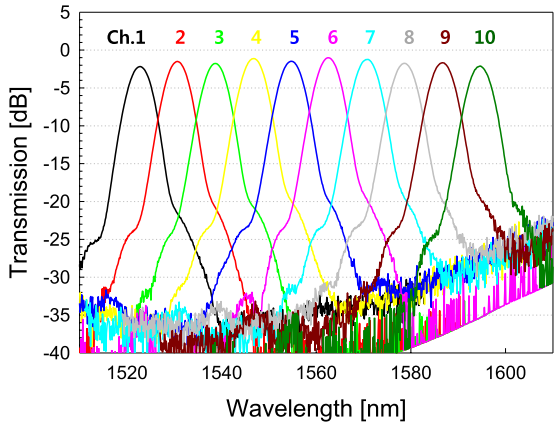

Fig. 2. Measured transmission spectra of the fabricated AWG. The transmission spectra were obtained using a broadband light source.

sub-assembly module, the FPCB has an arc-bent shape in the form of a grounded coplanar waveguide (GCPW) [7].

The AWG was designed and fabricated using the following parameters: an index contrast Δ of 2%, a core width and height of 3.8 μm, an array waveguide number of 50, a phase order of 13, a grating path difference of about 13.87 μm, a free propagation region (FPR) focal length of about 774.7 μm, and a total size of 8 mm $\times$ 2.5 mm. To realize a transmission response with a wide spectral width, tapered waveguides with a width of 4.5 μm, and a parabolic waveguide with a width of 7.5 μm, were designed at ten input ports of the input FPR and one output port of the output FPR using 7.5-μm tapered array waveguides, respectively.

For fabrication of the DFB-LDA, the epitaxial layers were grown using a lateral-flow-type metal-organic chemical vapor deposition (MOCVD). The layer stack before the SAG process consists of an n-InP buffer, a grating layer (band-gap wavelength $\lambda_{bg} = 1.35$ μm), n-InP space layer, and an outer separate confinement hetero-structure (SCH) layer ($\lambda_{bg} = 1.08$ μm). Nearly rectangular-shaped gratings with different periods were formed through E-beam direct-writing and dry-etching. Especially, in this work, in order to prevent the reduction of grating coupling coefficient caused by the increase in thickness and refractive-index of the SAG layer [7], grating duty was increased 25% to 50% with the increase of channel number. The mask patterns used for the SAG (material: SiN_x, thickness: 150 nm) have bilaterally symmetric shapes with a unit cell period of 500 μm. The spacing between adjacent mask stripes within the unit cell is the same as the opening width. Ten SAG mask patterns with different opening widths were designed to position the gain spectrums near the specified channel wavelengths. After the mask-patterning, the InGaAsP SAG layers were consecutively grown at the temperature of 630 °C and the pressure of 100 mbar as follows: a lattice-matched 20-nm thick inner SCH layer with a λ_{bg} of 1.24 μm, 7-pairs of QWs (i.e., 0.6% compressively strained 5-nm thick wells of 1.62 μm, and 0.45% tensile-strained 6-nm thick barrier of 1.3 μm), and a lattice-matched 20-nm thick inner SCH layer of 1.24 μm. After the removal of the SAG mask, an outer SCH layer, a p-InP residual cladding layer, a p-InGaAsP etch-stop layer, a p-InP upper cladding layer, and a p+InGaAs layer were grown in sequence.

RM-RWGs with a ridge-neck width of about 2.2 μm were fabricated. After typical LD fabrication processes, both facets of 300 μm long DFB-LDA chip bars were anti-reflection (AR) coated and their reflectivities were measured to be about 0.53% at a wavelength of 1.55 μm. The fabricated DFB-LDA was die-bonded on a metalized Si sub-mount, and then tested on the sub-assembly in the same manner as our previous work [7]. In order to examine the reflection immunity, we conducted the back-reflection test by using a circulator and an attenuator. For this test, there was no considerable change in the side mode suppression ratio (SMSR) as long as the feedback ratio (including double single-mode fiber (SMF) coupling losses, 2 $\times$ 5 dB) was in the test range of $\sim$5%. As the feedback ratio increases, the lasing spectrum began to be shifted slightly (within the wavelength range of 0.1 nm) from 0.1% and then become broadened abruptly from about 2% (for ch. 1). It was found that the coupling coefficient of DFB-LD is a critical parameter to have immunity for the back-reflection and a high coupling coefficient is preferred. On the other hand, for the fabricated DFB-LDA, even though the grating duty was increased with the increase of channel number, the reduction of coupling coefficient was not compensated sufficiently (i.e., the threshold current difference of about 10mA was obtained for all channels).

III. Experimental Results

The mounted DFB-LDA was actively aligned to the AWG. Through this alignment, the power of the AWG output port was detected using multi-mode fiber (MMF) with a coupling loss of about 0.5 dB. Fig. 2 shows the measured transmission spectra of the fabricated AWG. The AWG (insertion) loss and cross-talk level are 1 to 2.4 dB and about -20 dB at the channel center for all channels, respectively. The detailed measurement data are listed in Table I. For the active-alignment between the AWG and DFB-LDA, we first measured the output power of each DFB channel at a current of 90 mA, and after their active-alignment, measured the MMF-coupled power of the AWG at the same current. By comparing both output powers, the total losses for chs. 1, 4, 6, and 8 were measured to be 9, 7.4, 7.8, and 8.9 dB, respectively. For these data, the total loss can

TABLE I
MEASURED DATA OF AWG

Ch.	Peak wavelength [nm]	AWG loss [dB]	-1dB spectral width [nm]	-3dB spectral width [nm]
1	1522.764	2.38	2.94	5.10
2	1530.623	1.64	2.86	4.97
3	1538.701	1.88	2.88	5.00
4	1546.761	1.28	2.99	5.15
5	1554.738	1.57	3.01	5.14
6	1562.528	1.04	2.90	5.03
7	1570.731	1.40	3.00	5.15
8	1578.615	1.91	3.07	5.22
9	1586.645	1.69	2.96	5.14
10	1594.548	2.24	2.89	5.07

TABLE II
MEASURED LOSSES OF ACTIVE-ALIGNMENT BETWEEN DFB-LDA AND AWG

Ch.	Total loss [dB]	AWG loss [dB]	MMF loss [dB]	Align. losses [dB]	Deviation from AWG-peak [dB]	Extracted coupling loss [dB]
1	9	2.38	0.5	0.6	1.7	3.82
4	7.4	1.28	0.5	0.27	0.47	4.88
6	7.8	1.04	0.5	0.38	0.12	5.76
8	8.9	1.91	0.5	0.49	0.07	5.93

be assumed to consist of AWG loss (which can be obtained from Table I), MMF-coupling loss (0.5 dB), alignment losses (obtained from the power difference before and after the UV and thermal curing processes), lasing wavelength deviation from the AWG peak wavelength (obtained from the lasing wavelength and Table I), and coupling loss between the DFBA and AWG (extracted by subtracting the respective losses from the total loss in Table II). Consequently, it appears that when the number of channels increases, coupling loss (between the DFBA and AWG) increases. This result may be due to the bowed chip bar during the LD processes (e.g., BCB curing and lapping). Nevertheless, we note here that as the number of channels increases, the thicknesses and refractive-indices of the SAG layers increase owing to the growth rate enhancement and Indium richness, respectively, and therefore the optical mode confined in this waveguide narrows vertically. As a result, this narrowed near-field pattern (i.e., broadened far-field pattern) can increase the coupling loss. To confirm this, we analyzed the optical modes for waveguide structures containing SAG layers. The calculations show an increase of about 8° in the full-width at half maximum of far-field pattern of ch. 10. From this result, we can conclude that one of the main reasons for the change in coupling loss with the channel is a variation of optical mode through an increase in the thickness and refractive-index of the SAG layer.

For the integrated module, the output spectra were measured from the output port of the AWG using SMF under an operating temperature of 25 °C. Fig. 3 shows the measured

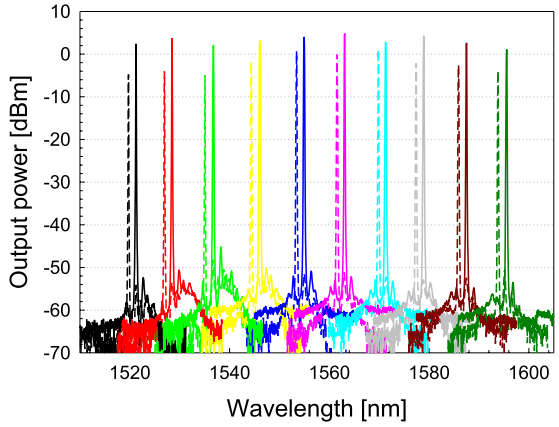

Fig. 3. Measured fiber-coupled output spectra measured from the output port of the AWG in the module at channel currents of 50 mA (dashed lines) and 100 mA (solid lines). The measurement was performed individually for all channels.

TABLE III
MEASURED PEAK WAVELENGTHS OF PACKAGED MODULE

Ch.	100 mA (static) [nm]	100 mA (modulation) [nm]	Deviation from AWG [nm]	Deviation from spec. [nm]
1	1521.12	1521.36	-1.40	-1.64
2	1528.48	1528.6	-2.02	-2.40
3	1536.68	1536.84	-1.86	-2.16
4	1546.08	1546.2	-0.56	-0.80
5	1554.96	1555.04	0.30	0.04
6	1563.08	1563.2	0.67	0.20
7	1571.32	1571.4	0.67	0.40
8	1578.84	1578.9	0.29	-0.10
9	1587.48	1587.56	0.91	0.56
10	1595.56	1595.6	1.05	0.60

lasing spectra at channel currents of 50 mA (dashed lines) and 100 mA (solid lines). The spectra show the SMSRs of >45 dB with an average channel spacing of about 8 nm. The AWG transmissions are shown at the bottom levels of the spectra. Relatively large peak-wavelength deviations between the DFB-LD and AWG are shown in chs. 1 through 4. For this device, it is possible to operate at a lower bias current by increasing the operating temperature. However, it is basically more desirable to implement a tuning element such as a micro-heater [14] at each of the DFB-LDA channels. Based on this static result, direct modulation was performed under a bias current of 100 mA and modulation currents of $\sim\pm 20$ mA. During the modulation test, there were additional shifts in the peak-wavelength of each channel shift (to a longer wavelength side) owing to the modulation current. The detailed measurement results are listed in Table III.

Fig. 4 shows the measured eye patterns at the back-to-back (BtoB) and after a 2-km transmission for each channel. The measurement was performed individually for all channels. The eye patterns are clearly opened with minimum dynamic extinction ratios (DERs) of 4.82 dB and 4.41 dB for before

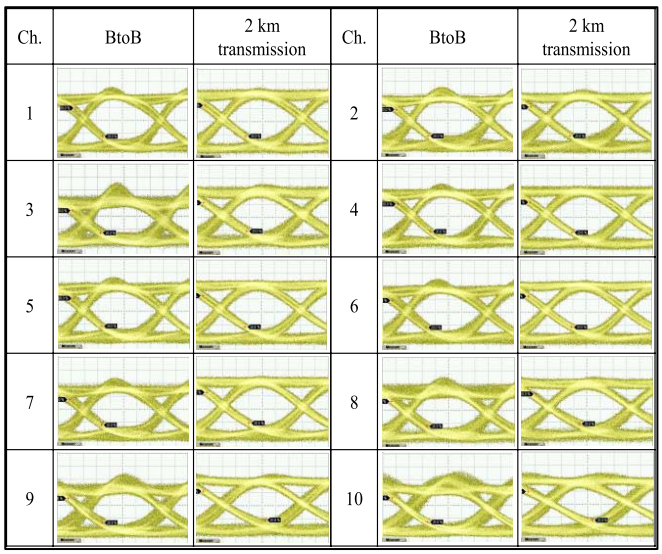

Fig. 4. Measured eye patterns at the back-to-back (BtoB) and after 2-km transmission for each channel. The measurement was performed individually for all channels. The signal pattern shows a PRBS of $2^{31}-1$. The bias and modulation currents are 100 mA and $\sim \pm 20$ mA, respectively.

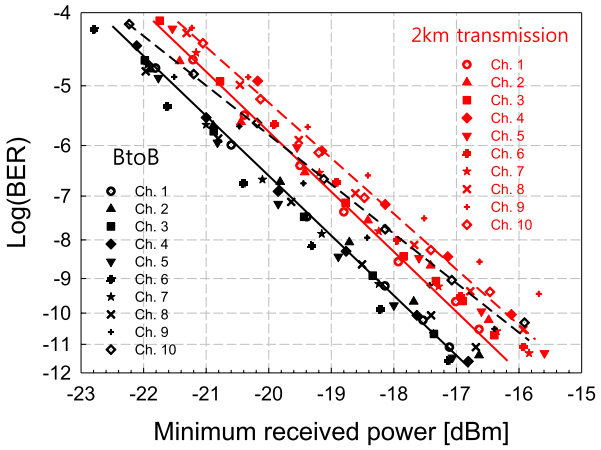

Fig. 5. BER link performances of ten channels at the back-to-back (black) and after a 2-km transmission (red) with respect to the minimum received power. The solid and dashed lines denote the BER performances of ch. 1 and ch. 10, respectively.

and after the transmission, respectively. However, in chs. 8 through 10, large amount of signal jitter and excursion appear at the BtoB. For this result, we think this is closely related to the increased back-reflection effect which results from the relatively lowered feedback immunity (caused by low coupling coefficient) and the relatively increased reflection between DFBA and AWG (caused by high coupling loss) and, as a result, this effect results in the degradation of signal quality (i.e. increase of noise) at the BtoB. Fig. 5 shows the BER link performance through 2-km of SMF fiber with respect to the minimum received power. A BER of 1^{-9} was shown for each of the ten wavelength channels. The minimum received powers at a BER of 1^{-9} were shown to be less than -18 dBm, except for ch. 9 (-17.6 dBm) and ch. 10 (-17.2 dBm), at the BtoB, and increased with a power penalty of <1.5 dB after the transmission. For the small transmission penalty of ch. 10, it can be explained by the reduction of noise (i.e., jitter and shading) of during the transmission. For example, the peak-to-peak jitters of ch. 10 at BtoB and 2km transmission were measured to be 30.61 and 24.27 ps, respectively.

IV. Summary

We developed a 10×10 Gb/s DFB-LDA integrated with a PLC-based AWG. For the fabricated AWG, an AWG loss of <2.4 dB and a -1 dB spectral width of about 3 nm were achieved for all channels. In an active-alignment test, the coupling loss between the DFBA and AWG was estimated to be <6 dB. For the AWG-integrated DFB-LDA, an SMSR of >45 dB and a peak wavelength deviation (from AWG) of <2 nm were obtained for each channel. The developed module showed a clear eye-opening with a DER of >4.4 dB and a power penalty of <1.5 dB after the 2-km transmission for all channels. Based on these results, we concluded that our DFB-LDA is capable of operating at a data rate of 10 Gb/s, and can be used as a low-cost light source for 100-Gb/s Ethernet transceivers. Additional improvements in the channel performance uniformity, wavelength controllability, and long-reach transmission will be the subjects of future investigations.

References

[1] *IEEE 802.3ba 40 Gb/s and 100 Gb/s Ethernet Task Force Public Area*. (Jun. 2010). [Online]. Available: http://www.ieee802.org/3/ba/index.html

[2] *10×10 Low Cost 100Gb/s Pluggable Optical Transceiver*. [Online]. Available: http://10x10msa.org/documents.htm, accessed Aug. 2, 2012.

[3] C. E. Zah *et al.*, "Monolithic integration of multiwavelength compressive-strained multiquantum-well distributed-feedback laser array with star coupler and optical amplifiers," *Electron. Lett.*, vol. 28, no. 25, pp. 2361–2363, Dec. 1992.

[4] R. Nagarajan *et al.*, "Large-scale photonic integrated circuits," *IEEE J. Sel. Topics Quantum Electron.*, vol. 11, no. 1, pp. 50–65, Jan./Feb. 2005.

[5] C. Zhang, S. Liang, H. Zhu, L. Han, and W. Wang, "Multichannel DFB laser arrays fabricated by upper SCH layer SAG technique," *IEEE J. Quantum Electron.*, vol. 50, no. 2, pp. 92–97, Feb. 2014.

[6] T. Schrans *et al.*, "100Gb/s 10km link performance of 10×10Gb/s hybrid approach with integrated WDM array of DFB lasers," in *Proc. OFC/NEOEC*, 2009, pp. 1–3, paper NThA4.

[7] O. K. Kwon, Y. A. Leem, Y. T. Han, C. W. Lee, K. S. Kim, and S. H. Oh, "A 10×10 Gb/s DFB laser diode array fabricated using a SAG technique," *Opt. Exp.*, vol. 22, no. 8, pp. 9073–9080, Apr. 2014.

[8] O. K. Kwon, K. H. Kim, E. D. Sim, J. H. Kim, H. S. Kim, and K. R. Oh, "Broadly wavelength-tunable external cavity lasers with extremely low power variation over tuning range," *IEEE Photon. Technol. Lett.*, vol. 17, no. 3, pp. 537–539, Mar. 2005.

[9] J. H. Song, K. Kim, Y. A. Leem, H. J. Kim, and G. Kim, "Strain-controlled selective-area growth of InGaAsP films on InP," *Jpn. J. Appl. Phys.*, vol. 46, no. 33, pp. L783–L785, 2007.

[10] O.-K. Kwon, K.-S. Kim, J.-S. Sim, and Y.-S. Beak, "Operational properties of ridge waveguide lasers with laterally tapered waveguides for monolithic integration," *ETRI J.*, vol. 29, no. 6, pp. 811–813, Dec. 2007.

[11] S. H. Oh, O. K. Kwon, K.-H. Yoon, K. S. Kim, and O.-K. Kwon, "Superluminescent diode with circular beam shape," *IEEE Photon. Technol. Lett.*, vol. 25, no. 23, pp. 2289–2291, Dec. 1, 2013.

[12] O. K. Kwon, Y. A. Leem, D. H. Lee, C. W. Lee, Y. S. Baek, and Y. C. Chung, "Effects of asymmetric grating structures of output efficiency and single longitudinal mode operation in $\lambda/4$-shifted DFB laser," *IEEE J. Quantum Electron.*, vol. 47, no. 9, pp. 1185–1194, Sep. 2011.

[13] Y. T. Han *et al.*, "A cost-effective 25-Gb/s EML TOSA using all-in-one FPCB wiring and metal optical bench," *Opt. Exp.*, vol. 21, no. 22, pp. 26962–26971, Oct. 2013.

[14] N. Kim *et al.*, "Widely tunable 1.55-μm detuned dual-mode laser diode for compact continuous-wave THz emitter," *ETRI J.*, vol. 33, no. 5, pp. 810–813, Oct. 2011.